Pergamon

Int. J. Heat Mass Transfer. Vol. 37, No. 7, pp. 1123–1132, 1994

0017-9310/94 $6.00 + 0.00

0017-9310(93)E0028-F

The effect of mass transfer on Kelvin–Helmholtz instability at the gas–liquid interface of a sonic reacting and non-reacting gas jet submerged in a liquid

S. H. CHAN, Y. S. WANG and C. C. TAN

Department of Mechanical Engineering, University of Wisconsin–Milwaukee, P.O. Box 784, Milwaukee, WI 53201, U.S.A.

(*Received* 21 *April* 1993 *and in final form* 27 *October* 1993)

Abstract—The theory of Kelvin–Helmholtz instability is employed to analyze the instability phenomena of non-reacting and reacting stratified gas flows injected sonically into a liquid. The effect of the mass transfer at the gas–liquid interface on the instability is investigated. It is shown that the mass transfer affects the pressure perturbation which acts to transfer energy from the gas phase to the liquid layer through its evaporating and condensing behavior, its wave-drag and lift components, against forces due to surface tension and liquid viscosity. The dimensionless wave frequency, amplification, and wavelength at the maximum instability are presented as a function of a dimensionless surface tension/viscous parameter and a blowing parameter due to the interfacial mass transfer. The interfacial evaporation is found to enhance the instability while the interfacial condensation is to reduce the instability. The results provide the theoretical explanation of the reported dynamic and instability behavior found in the reacting jet of a HCl gas submerged in the ammonia aqueous solution. Finally, an application to the prediction of the break-off plume length observed in submerged reacting jets is presented and the results are compared to experimental data of the HCl(g)–NH_3(aq) system.

1. INTRODUCTION

SUBMERGED turbulent reacting jets are of interest in a number of applications. In stored chemical energy propulsion systems for underwater applications, a gaseous sulfur hexafluoride gas is injected at a choked speed into a liquid lithium bath in a reactor [1–5]. The reaction forms a complex submerged turbulent jet and releases relatively high heat of reaction as a heat source to power a Rankine cycle for underwater propulsion. Similarly, submerged reacting jets are widely used in the basic oxygen steel making process [6] and in steam generator safety analyses (steam jets submerged in liquid sodium) of liquid metal-cooled reactors [7], etc.

In these applications, the opaqueness of the liquid metals and their container makes flow visualization of the submerged reacting jets difficult. Recently, Cho *et al.* [8] have circumvented the experimental difficulty by selecting an optically transparent pair of reactants, namely, by injecting a HCl gas (oxidant) at a choked speed into an aqueous ammonia solution (fuel). In a series of experiments by varying the underexpansion ratio and the concentration of ammonia (fuel) in the solution, their experiments revealed an unexpected and unexplained phenomenon in submerged reacting jets, namely, instability occurred when ammonia was present in the solution. In fact the instability was so severe that plume break-off occurred periodically near the orifice exit and the bath pressure experienced large periodic fluctuations as well. This instability is of concern as in any propulsion system, but has not been investigated analytically.

Several investigators have studied both experimentally and analytically the Kelvin–Helmholtz instability of the gas–liquid interface. Chang and Russel [9] analyzed the case where a subsonic and a supersonic gas jet flowed through a plane of liquid. Nachtsheim [10] examined the three-dimensional disturbance of a shear flow in which a thin liquid film was exposed to a supersonic gas stream with wave fronts obliqued to the external stream. Nayfeh and Saric [11] analyzed a compressible gas stream flowing over a liquid under the influence of a body force directed outward from or toward the liquid. Craik [12] examined both experimentally and analytically the instability of thin liquid films exposed to an incompressible air stream. Chawla [13] analyzed the case where a subsonic or a sonic gas jet is flowing through a liquid, under the action of pressure perturbation, liquid viscosity, and surface tension. Chawla [14] also developed a simple model for the rate of entrainment of the liquid in accordance to the knowledge of Kelvin–Helmholtz instability of the interfacial wave. None of them has considered the instability of a gas–liquid interface with mass transfer and is applicable to the present submerged reacting jet, such as the reacting hydrochloride–aqueous ammonia system in which a periodic or cyclic plume behavior was found. The present analysis explores the theoretical background in understanding the Kelvin–Helmholtz instability of a liquid–vapor interface with mass transfer

NOMENCLATURE

a	radius of gas jet
A	nondimensional empirical constant
B	driving force
c	sonic velocity at any local point in the jet
C_0	dimensionless empirical constant
C_L	an empirical constant
C_p	dimensionless pressure coefficient
D	enthalpy empirical constant
h	enthalpy
l	$l_r - il_i$
L_0	break-off length of the gas stream
m_i	mass fraction of i species
M_i	molecular weight of i species
$\dot{m}$	evaporation or condensation flux
P_1	viscosity parameter
P_2	fictitious diffusion parameter
P	pressure
r	radial coordinate
t	time
T	temperature
U_g	velocity of the gas at the orifice
V_1	blowing velocity at interface
V_x	axial velocity of gas jet
V_r	radial velocity of gas jet
V_f	liquid velocity at/normal to interface
V_g	gas velocity at/normal to interface.

Greek symbols

α	complex angular frequency
α_r	time amplification factor [s^{-1}]
α_i	angular frequency [s^{-1}]
γ	specific heat ratio
η	radial displacement of gas–liquid interface from mean radius of the jet
η_0	amplitude of displacement at the orifice
κ	wave number, $2\pi/\lambda$
λ	wavelength [m]
μ	dynamic viscosity of liquid
ρ	density
σ	surface tension
ϕ_g	velocity potential
ϕ	dimensionless perturbation potential
ψ	stream function
ω	wave velocity vs orifice gas velocity.

Superscripts

0	stagnation quantity
*	dimensionless quantity.

Subscripts

f	liquid
g	gas
m	maximum instability
o	orifice.

(blowing velocity) across the interface. Solution of Kelvin–Helmholtz instability analysis is then used, as an application, to determine the break-off distance of submerged reacting jets and the results of the prediction are compared to the reported data of HCl(g)–NH_3(aq) jets [8].

2. GOVERNING EQUATIONS FOR THE REACTING GAS JETS

Figure 1 illustrates a submerging sonic gas jet in an infinite mass of liquid with a uniform axial velocity of U_g, namely the sonic velocity at the nozzle throat. Similar to the prior works (e.g. [13]), the gas jet is assumed without loss of generality to have a mean radius equal to the orifice radius, a. Furthermore, the gas is treated as an ideal frictionless fluid and the short wave approximation, which reduces the problem of two-dimensional axisymmetric jet to that of two-dimensional planar jet, is employed. However, a mass suction or blowing at the jet's gas–liquid interface is considered to simulate a reaction between the gas and the surrounding reactive fluid. The suction and blowing can also simulate respectively condensation and evaporation processes at the interface. In view of the above assumptions, if the flow field is assumed free from shock waves of finite strength and body forces, the gas flow can be considered an isentropic flow, and the flow field can be considered by the potential flow theory. The hydrodynamic equations governing the gas motion in an axisymmetric coordinate system are

$$\frac{\partial \rho}{\partial t} + \rho\left[\frac{1}{r}\frac{\partial (rV_r)}{\partial r} + \frac{\partial V_x}{\partial x}\right] + V_x\frac{\partial \rho}{\partial x} + V_r\frac{\partial \rho}{\partial r} = 0 \quad (1)$$

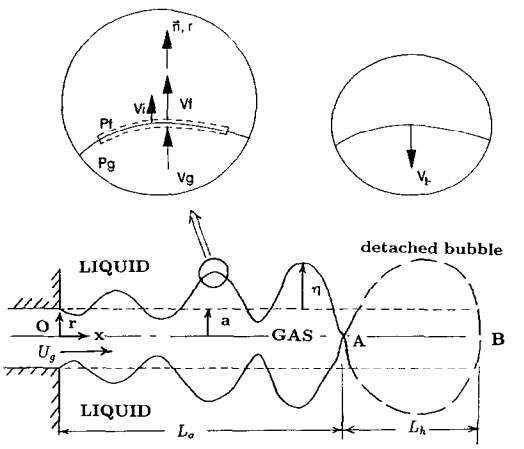

FIG. 1. Schematic diagram of reacting gas jet submerged in liquid—linearized treatment in the analysis.

$$\frac{\partial V_x}{\partial t}+V_x\frac{\partial V_x}{\partial x}+V_r\frac{\partial V_x}{\partial r}=-\frac{1}{\rho}\frac{\partial P}{\partial x} \tag{2}$$

and

$$\frac{\partial V_r}{\partial t}+V_x\frac{\partial V_r}{\partial x}+V_r\frac{\partial V_r}{\partial r}=-\frac{1}{\rho}\frac{\partial P}{\partial r}. \tag{3}$$

Using the sound speed and the velocity potential equations

$$\frac{\mathrm{d}P}{\mathrm{d}\rho}=c^2 \tag{4}$$

$$V_x=\frac{\partial \phi_g}{\partial x}+U_g;\quad V_r=\frac{\partial \phi_g}{\partial r} \tag{5}$$

in equations (1)–(3) yields the nonlinear wave equation,

$$\frac{\partial^2\phi_g}{\partial t^2}+2\frac{\partial\phi_g}{\partial x}\frac{\partial^2\phi_g}{\partial x\,\partial t}+2\frac{\partial\phi_g}{\partial r}\frac{\partial^2\phi_g}{\partial r\,\partial t}+\left(\frac{\partial\phi_g}{\partial x}\right)^2\left(\frac{\partial^2\phi_g}{\partial x^2}\right)+2\frac{\partial\phi_g}{\partial x}\frac{\partial\phi_g}{\partial r}\frac{\partial^2\phi_g}{\partial r\,\partial x}+\left(\frac{\partial\phi_g}{\partial r}\right)^2\frac{\partial^2\phi_g}{\partial r^2}=c^2\left(\frac{\partial^2\phi_g}{\partial x^2}+\frac{\partial^2\phi_g}{\partial r^2}+\frac{1}{r}\frac{\partial\phi_g}{\partial r}\right). \tag{6}$$

To solve the above nonlinear equation, a local sonic velocity of the gas jet must be determined initially. Multiplying equations (6) and (7) by $\mathrm{d}x$ and $\mathrm{d}r$, respectively, adding the resulting equation and expressing in terms of ϕ_g yield

$$\mathrm{d}\left(\frac{\partial\phi_g}{\partial t}\right)+\frac{1}{2}\mathrm{d}\left(\frac{\partial\phi_g}{\partial x}\right)^2+\frac{1}{2}\mathrm{d}\left(\frac{\partial\phi_g}{\partial r}\right)^2=-\frac{1}{\rho}\mathrm{d}P.$$

For an isentropic flow along a streamline,

$$T\,\mathrm{d}S=0=\mathrm{d}h-\frac{1}{\rho}\mathrm{d}P.$$

Eliminating the pressure between the above two equations, integrating from a stagnation point ($h_o=C_pT_o+U_g^2/2$) to a downstream point ($h=C_pT$) and using $C_pT=c^2/(\gamma-1)$ yield the local sonic velocity of the gas jet,

$$c^2=(\gamma-1)\left[\frac{1}{2}U_g^2+\frac{c_o^2}{\gamma-1}-\frac{\partial\phi_g}{\partial t}-\frac{1}{2}\left(\frac{\partial\phi_g}{\partial x}\right)^2-\frac{1}{2}\left(\frac{\partial\phi_g}{\partial r}\right)^2\right] \tag{7}$$

where c_o is the sonic velocity at the orifice and γ is the ratio of specific heats.

It is worth noting here that the governing equations (6)–(7) for the gas jet are general and applicable to all regimes of the two-dimensional axisymmetric compressible potential flow. Without considering the expansion or contraction motion of the gas boundary due to the vaporization or condensation between the jet gas and the surrounding reactive liquid, the following kinematic boundary condition at the gas–liquid interface, i, must be satisfied,

$$\left(\frac{\partial\phi_g}{\partial r}\right)_i=\frac{\mathrm{d}\eta}{\mathrm{d}t}=\frac{\partial\eta}{\partial t}+\frac{\partial\eta}{\partial x}\frac{\mathrm{d}x}{\mathrm{d}t} \tag{8}$$

where η is the displacement of the gas–liquid interface from the mean jet radius (see Fig. 1). For non-reacting evaporating or condensing fluids, a blowing velocity (see V_l in Fig. 1) into the gas side relative to the interface velocity ($-V_l=V_{g,r}-V_{i,r}$) is introduced such that equation (8) becomes

$$V_{g,r}=\left(\frac{\partial\phi_g}{\partial r}\right)_i=-V_l+\frac{\partial\eta}{\partial t}+\frac{\partial\eta}{\partial x}\frac{\mathrm{d}x}{\mathrm{d}t} \tag{9}$$

where a positive value of V_l represents evaporation while a negative value means condensation. For reacting flows, the equivalent blowing velocity is properly estimated as shown later.

3. LINEARIZATION OF EQUATIONS OF MOTION FOR THE GAS PHASE

The gas phase velocity potential, ϕ_g, is expressed in terms of a dimensionless perturbation potential ϕ as

$$\phi_g(r,x,t)=U_gx-aV_l\ln r+\varepsilon_\phi U_g\lambda\phi(y^*,x^*,t^*) \tag{10}$$

where the term, $aV_l\ln r$, describes the contribution due to the presence of evaporation at the gas–liquid interface. For a planar flow, $aV_l\ln r$ is replaced by V_lr.

The dimensionless variables are defined as

$$x^*=\frac{x}{\lambda},\quad y^*=\frac{(a-r)\delta}{a}$$

$$t^*=w^*\left(\frac{tU_g}{\lambda}\right)=\frac{tU_g}{\lambda}\frac{|\alpha|\lambda}{2\pi U_g},\quad \eta^*(x^*,t^*)=\frac{\eta(x,t)}{\varepsilon a}$$

where λ is the disturbance wavelength, and α is the complex angular frequency of the interfacial wave. As presented by Chawla [13], the dimensionless parameters ε_ϕ, ε, ω^*, and δ are to be defined in a given neighborhood in such a way that ϕ, η^*, and their derivatives with respect to any of the dimensionless independent variables are of the order of unity. By differentiating equation (10) with respect to x, r, and t, respectively, the axial and radial velocities are

$$\frac{\partial\phi_g}{\partial x}=U_g(1+\varepsilon_\phi\phi_{x^*}) \tag{11}$$

$$\frac{\partial\phi_g}{\partial r}=-\frac{\delta}{\delta-y^*}V_l-\varepsilon_\phi U_g\frac{\lambda\delta}{a}\phi_{y^*}. \tag{12}$$

Similarly, the sound velocity given by equation (7) can be expressed as

$$c^2 = \frac{U_g^2}{M_o^2} - (\gamma-1)U_g^2\left[\frac{1}{2}\left(\frac{a}{r}\right)^2\frac{V_l^2}{U_g^2} + \varepsilon_\phi\left(\omega^*\phi_{t^*} + \frac{a}{r}\frac{V_l}{U_g}\frac{\delta\lambda}{a}\phi_{y^*y^*} + \phi_{x^*}\right)\right] - (\gamma-1)U_g^2\frac{1}{2}\varepsilon_\phi^2\left[\phi_{x^*}^2 + \left(\frac{\lambda\delta}{a}\right)^2\phi_{y^*}^2\right]. \quad (13)$$

where $M_o = U_g/c_o$ and ϕ_{x^*} is the derivative of ϕ with respect to x^*, etc.

Pressure distributions are quoted in terms of the nondimensional pressure coefficient C_p. Since the flow through an expansion wave is, as suggested earlier, isentropic, the use of the isentropic pressure and temperature relations and the sound velocity of equation (13) yields

$$C_p = \frac{P_g - P_o}{0.5P_gU_g^2} = \frac{2}{\gamma M_o^2}\left\{\left[1-(\gamma-1)M_o^2\left(\frac{1}{2}\left(\frac{a}{r}\right)^2\frac{V_l^2}{U_g^2} + \varepsilon_\phi\omega^*\phi_{t^*} + \varepsilon_\phi\phi_{x^*} + \frac{aV_l}{rU_g}\frac{\delta\lambda}{a}\phi_{y^*}\varepsilon_\phi + \frac{1}{2}\varepsilon_\phi^2\phi_{x^*}^2 + \frac{1}{2}\varepsilon_\phi^2\left(\frac{\lambda\delta}{a}\right)^2\phi_{y^*}^2\right)\right]^{\gamma/(\gamma-1)} - 1\right\}. \quad (14)$$

Finally, upon the substitution of the velocity potential equation (10) and the sound velocity equations (13) into the wave equations (6) yields readily

$$\left(\frac{M_o}{\delta}\right)^2\left(\frac{\omega^* a}{\lambda}\right)^2\phi_{t^*t^*} + 2\left(\frac{M_o}{\delta}\right)^2\omega^*\left(\frac{a}{\lambda}\right)^2\phi_{x^*t^*} + 2\left(\frac{M_o}{\delta}\right)^2\omega^*\left(\frac{a}{\lambda}\right)^2\varepsilon_\phi\phi_{x^*}\phi_{x^*t^*} + 2M_o^2\omega^*\frac{a}{\lambda} \times \frac{1}{\delta-y^*}\frac{V_l}{U_g}\phi_{y^*t^*} + 2M_o^2\omega^*\frac{a}{\lambda}\left(\varepsilon_\phi\frac{\lambda}{a}\phi_{y^*}\right)\phi_{y^*t^*} + \frac{M^2}{\delta^2}\left(\frac{a}{\lambda}\right)^2\varepsilon_\phi^2\phi_{x^*}^2\phi_{x^*x^*} + 2M_o^2\frac{a}{\lambda}\left(\frac{1}{\delta-y^*}\frac{V_l}{U_g} + \varepsilon_\phi\frac{\lambda}{a}\phi_{y^*} + \varepsilon_\phi^2\phi_{x^*}\frac{\lambda}{a}\phi_{y^*}\right)\phi_{x^*y^*} + \frac{M_o^2}{\delta^2\varepsilon_\phi}\frac{a^2}{\lambda}\left[\frac{\delta^2}{(\delta-y^*)^2}\frac{V_l^2}{U_g}\frac{\delta^2}{(\delta-y^*)^2}\frac{V_l}{aU_g} + 2\left(\frac{\delta}{\delta-y^*}\frac{V_l}{U_g}\right)\left(\frac{\delta^2}{(\delta-y^*)^2}\frac{V_l}{aU_g}\right)\varepsilon_\phi\frac{\delta\lambda}{a}\phi_{y^*}\right] + \frac{M_o^2}{\delta^2\varepsilon_\phi}\frac{a^2}{\lambda} \times \left[\frac{\delta^2}{(\delta-y^*)^2}\frac{V_l^2}{U_g^2}\varepsilon_\phi\frac{\delta^2\lambda}{a^2}\phi_{y^*y^*}\right] + \frac{M_o^2}{\delta^2\varepsilon_\phi}\frac{a^2}{\delta} \times \left(\varepsilon_\phi^2\left(\frac{\delta\lambda}{a}\right)^2\phi_{y^*}^2\frac{\delta^2}{(\delta-y^*)^2}\frac{V_l}{aU_g}\right) + \frac{M_o^2}{\delta^2\varepsilon_\phi}\frac{a^2}{\lambda} \times \left[2\frac{\delta}{\delta-y^*}\frac{V_l}{U_g}\varepsilon\frac{\partial\lambda}{a}\phi_{y^*}\varepsilon_\phi\frac{\delta^2\lambda}{a^2}\phi_{y^*y^*} + \varepsilon_\phi^2\left(\frac{\delta\lambda}{a}\right)^2 \times \phi_{x^*}^2\varepsilon_\phi\frac{\delta^2\lambda}{a^2}\phi_{y^*y^*}\right] = \frac{1}{\varepsilon_\phi}\frac{a^2}{\lambda}\frac{M_o^2}{\delta^2}(\gamma-1) \times \left[\frac{1}{M_o^2}\left(\frac{\varepsilon_\phi}{\lambda}\phi_{x^*x^*} + \varepsilon_\phi\frac{\delta^2\lambda}{a^2}\phi_{y^*y^*} - \varepsilon_\phi\frac{\delta^2\lambda}{a^2(\delta-y^*)}\phi_{y^*}\right)\right] - \frac{1}{\varepsilon_\phi}\frac{a^2}{\lambda}\frac{M_o^2}{\delta^2}(\gamma-1)\left[\frac{\delta^2}{2(\delta-y^*)^2}\frac{V_l^2}{U_g^2} + \varepsilon_\phi\left(\omega^*\phi_{t^*} + \phi_{x^*} + \frac{\delta}{\delta-y^*}\frac{V_l}{U_g}\varepsilon_\phi\frac{\delta\lambda}{a}\phi_{y^*}\right)\right] - \frac{1}{\varepsilon_\phi}\frac{a^2}{\lambda}\frac{M_o^2}{\delta^2}(\gamma-1)\left[\frac{1}{2}\varepsilon_\phi^2\left(\phi_{x^*}^2 + \frac{\delta^2\lambda^2}{a^2}\phi_{y^*}^2\right)\right] \times \left(\frac{\varepsilon_\phi}{\lambda}\phi_{x^*x^*} + \varepsilon_\phi\frac{\delta^2\lambda}{a^2}\phi_{y^*y^*} - \varepsilon_\phi\frac{\delta^2\lambda}{a^2(\delta-y^*)}\phi_{y^*}\right). \quad (15)$$

The theory of small perturbation requires that the deviations of the velocity components and the pressure from the reference conditions be small. As a result, from equations (11)–(14), we obtain the following conditions:

$$\varepsilon_\phi \ll 1, \quad \varepsilon_\phi\frac{\delta\lambda}{a} \ll 1, \quad \varepsilon_\phi M_o^2 \ll 1$$

$$\varepsilon_\phi M_o^2\omega^* \ll 1, \quad \left(\varepsilon_\phi M_o\frac{\delta\lambda}{a}\right) \ll 1. \quad (16)$$

In the subsequent analysis, two practical cases are of physical relevance to the present problem of concerns.

The first case under consideration is that wave velocity $|\alpha|\lambda/2\pi$ is much less than the gas velocity U_g,

$$\omega^* = O(\varepsilon_p) = \frac{|\alpha|\lambda}{2\pi U_g} \ll 1. \quad (17)$$

Applying the conditions specified by equation (16) and the sonic flow condition, $M_o = 1$, into equation (15) results in

$$\phi_{y^*y^*} - \frac{1}{\delta-y^*}\phi_{y^*} = (\gamma+1)\phi_{x^*}\phi_{x^*x^*} + 2\frac{\omega^*}{\varepsilon_\phi}\phi_{x^*t^*} + \frac{2}{\varepsilon_\phi}\frac{1}{\delta-y^*}\frac{V_l}{U_g}\phi_{x^*y^*}. \quad (18)$$

If a linearized solution to the nonlinear equations of motion for the gas phase is desired for short waves, i.e. for $\lambda/a \ll 1$, we expand ϕ_g in a power series in λ/a. From equation (10), it implies $\varepsilon_\phi = \lambda/a$. Similar to Chawla [13], by setting $1/\delta^2(a/\lambda)^2\varepsilon_\phi = 1$ and using $\varepsilon_\phi = \lambda/a$, the expression of δ is found as $\delta = (a/\lambda)^{1/2}$. Thus, when $\lambda/a \ll 1$, we obtain $\delta \gg 1$ and equation (18) is simplified to

$$\phi_{y^*y^*} = (\gamma+1)\phi_{x^*}\phi_{x^*x^*} + 2\frac{\omega^*}{\varepsilon_\phi}\phi_{x^*t^*}. \quad (19)$$

However, if $\omega^* \gg \varepsilon_\phi$ but $\omega^* \ll 1$ (case 1), and by setting $M_o = 1$ and $\omega^*/\delta^2 = (a/\lambda)^2 = 1$, equation (15) can be simplified into

$$\phi_{y^*y^*} = 2\phi_{x^*t^*}. \tag{20}$$

It is noted here that equations (19), (20) are given for two-dimensional planar flow since the condition $\delta \gg 1$ has been used in the simplification.

As to the kinematic boundary condition for the gas jet given by equation (9), after substituting the radial velocity by equation (12) and expressing η in terms of $\eta^* \equiv \eta/\varepsilon a$, it yields

$$-\frac{a}{r}V_1\frac{\lambda}{aU_g} - \varepsilon_\phi\delta\left(\frac{\lambda}{a}\right)^2\phi_{y^*} = -V_1\frac{\lambda}{aU_g} + \varepsilon(\omega^*\eta_{t^*}^* + \eta_{x^*}^*(1+\varepsilon_\phi\phi_{x^*})). \tag{21}$$

For two-dimensional planar flow approximation, $a \approx r$, and applying the first condition of equation (16) (small perturbation theory), the condition given by equation (17), and the fact that $\delta\varepsilon_\phi(\lambda/a^2) = \varepsilon$ for case 1 [13], the above is simplified to

$$-\phi_{y^*} = \eta_{x^*}^*. \tag{22}$$

As to C_p, the term $(a/r)(V_1/U_g)\varepsilon_\phi(\delta\lambda/a)\phi_{y^*}$ in equation (14) cannot be neglected for it is greater than the second order small quantity. We have acknowledged that, for case 1 of the present discussion, $\omega^* \ll 1$, $V_1/U_g \ll 1$, $\varepsilon_\phi \ll 1$, and $(\delta\lambda/a)^2 \approx 1/\varepsilon_\phi$. As a result of these inequalities, we can conclude that $\varepsilon_\phi^3 \ll 1$ and $\varepsilon_\phi^2 \ll 1$. Then the pressure-coefficient is simplified to

$$C_p = \frac{2}{\gamma M_o^2}\left\{\left[1-(\gamma-1)M_o^2\varepsilon_\phi \times\left(\phi_{x^*} + \frac{aV_1\delta\lambda\phi_{y^*}}{rU_g a}\right)\right]^{\gamma/(\gamma-1)} - 1\right\}.$$

Binomial series expansion and a neglect of terms of smaller order yields an even simpler expression,

$$C_p = -2\varepsilon_\phi\left(\phi_{x^*} + \frac{V_1}{U_g}\left(\frac{\delta\lambda}{a}\right)\phi_{y^*}\right). \tag{23}$$

The above analysis has indicated that the transient component of gas motion dominates over other terms in equation (18), and, as a result, the governing equation (20) becomes linear, and the boundary conditions and pressure coefficient have simplified to equations (22) and (23) respectively.

Case 2 deals with the situation where the wave velocity is of the same order of magnitude as the gas velocity,

$$\omega^* = \frac{|\alpha|\lambda}{2\pi}\frac{1}{U_g} = O(1). \tag{24}$$

Similarly, under the short wave approximation as well as using the small perturbation theory and the sonic flow condition, equation (15) is simplified to

$$\phi_{y^*y^*} = \omega^*\phi_{t^*t^*} + 2\phi_{x^*t^*} \tag{25}$$

where, similar to Chawla [13], the choice of $(\omega^*/\delta^2)(a/\lambda)^2 = 1$ was made. Also, the boundary condition given by equation (9) becomes

$$-\phi_{y^*} = \omega^*\eta_{t^*}^* + \eta_{x^*}^* \tag{26}$$

and the pressure coefficient C_p given by equation (14) becomes

$$C_p = -2\varepsilon_\phi(\omega^*\phi_{t^*} + \phi_{x^*}) - 2\varepsilon_\phi\frac{a}{r}\frac{V_1}{U_g}\left(\frac{\delta\lambda}{a}\right)\phi_{y^*}. \tag{27}$$

Since governing equations (25)–(27) of case 2 embrace the governing equations (20), (22), and (23) of case 1 under the more general condition of $\omega^* = O(1)$, the same short wave approximation and the same theory of small perturbation, we therefore use only equations (25)–(27). After transforming equations (25)–(26) into dimensional forms for a planar gas flow ($a \approx r$), they yield

$$\frac{\partial^2\phi_g}{\partial r^2} - \frac{2}{U_g}\frac{\partial^2\phi_g}{\partial t\,\partial x} - \frac{1}{U_g^2}\frac{\partial^2\phi_g}{\partial t^2} = 0 \tag{28}$$

$$\frac{\partial\phi_g}{\partial r} = -V_1 + \frac{\partial\eta}{\partial t} + U_g\frac{\partial\eta}{\partial x} \quad \text{at} \quad r = a. \tag{29}$$

The downstream pressure in the gas jet can be obtained from equation (27) by noting that $P_o = \rho_g U_g^2/\gamma$,

$$P_g = \frac{\gamma+1}{\gamma}\rho_g U_g^2 - \rho_g\left(\frac{\partial\phi_g}{\partial t} + U_g\frac{\partial\phi_g}{\partial x}\right) + \rho_g V_1^2 + \rho_g V_1\frac{\partial\phi_g}{\partial r}. \tag{30}$$

4. GOVERNING EQUATIONS FOR THE LIQUID PHASE

The linearized equations of the motion of liquid consistent with the short-wave approximation are

$$\frac{\partial U}{\partial x} + \frac{\partial V}{\partial r} = 0 \tag{31}$$

$$\frac{\partial U}{\partial t} = -\frac{1}{\rho}\frac{\partial P}{\partial x} + \nu\left(\frac{\partial^2 U}{\partial x^2} + \frac{\partial^2 U}{\partial r^2}\right) \tag{32}$$

and

$$\frac{\partial V}{\partial r} = -\frac{1}{\rho}\frac{\partial P}{\partial r} + \nu\left(\frac{\partial^2 V}{\partial x^2} + \frac{\partial^2 V}{\partial r^2}\right) \tag{33}$$

where U and V are the axial and the radial components of the induced motion of liquid, respectively. P is the pressure at any point in the liquid state, ν is the kinematic viscosity of the liquid, and ρ is the liquid's density.

The linearized kinematic boundary condition at the gas–liquid interface (on the liquid side) is

$$V = -\frac{\rho_{vap}}{\rho_f}V_1 + \frac{\partial\eta}{\partial t} \quad \text{at} \quad r = a. \tag{34}$$

In addition, the following dynamic boundary con-

ditions must also be satisfied by the solution: (a) continuity of tangential stress at the interface

$$\mu\left(\frac{\partial U}{\partial r}+\frac{\partial V}{\partial x}\right)=0 \tag{35}$$

and (b) continuity of normal stress at the gas–liquid interface.

The momentum balance of a control volume containing an evaporating interface moving with a velocity V_i as shown in Fig. 1 yields

$$\dot{m}_{\text{evap}}(V_g-V_f)+(P_g-P_f)+2\mu\frac{\partial V_{r,f}}{\partial r}=\frac{\sigma}{a}-\sigma\frac{\partial^2\eta}{\partial x^2} \tag{36}$$

where the evaporation rate,

$$\dot{m}_{\text{evap}}=\rho_g(V_g+V_i)=\rho_f(V_f+V_i). \tag{37}$$

Now, let us define a stream function $\psi(r,x,t)$ that will help us later in the analysis of wave propagation. The stream function is defined in such a way that the continuity equation (31) is satisfied.

To simplify equations (31)–(33), a stream function $\psi(r,x,t)$

$$U=\frac{\partial\psi}{\partial r};\quad V=-\frac{\partial\psi}{\partial x} \tag{38}$$

is introduced into equations (32), (33) to yield

$$\left(\nabla^2-\frac{1}{\nu}\frac{\partial}{\partial t}\right)\nabla^2\psi=0. \tag{39}$$

Since $(\nabla^2-(1/\nu)\,\partial/\partial t)$ and ∇^2 commute, the function ψ can be separated into two parts:

$$\nabla^2\psi_1=0 \tag{40}$$

$$\left(\nabla^2-\frac{1}{\nu}\frac{\partial}{\partial t}\right)\psi_2=0 \tag{41}$$

such that the general solution of equation (39) is given

$$\psi=\psi_1+\psi_2 \tag{42}$$

and equations (32), (33) are simplified to

$$\frac{1}{\rho}\frac{\partial P}{\partial x}=-\frac{\partial}{\partial t}\left(\frac{\partial\psi_1}{\partial r}\right) \tag{43}$$

$$\frac{1}{\rho}\frac{\partial P}{\partial r}=\frac{\partial}{\partial r}\left(\frac{\partial\psi_1}{\partial x}\right). \tag{44}$$

5. SOLUTIONS OF FLOW EQUATIONS

In the linearized stability analysis, the motion of the gas–liquid interface can be described in the following manner:

$$\eta(x,t)=\eta_o e^{i\kappa x+\alpha t} \tag{45}$$

where η_o is the initial amplitude, κ is the wavenumber, and α is the vector sum of time amplification factor (α_r) and the angular frequency of the disturbance (α_i).

As a consequence, the solution of the gas flow of equation (28), which satisfies the boundary condition of equation (29) under the planar approximation, is

$$\phi_g(r,x,t)=U_g x-V_i r+(\alpha+i\kappa U_g)\frac{\sin(K_c r)}{K_c\cos(K_c a)}\eta(x,t) \tag{46}$$

where

$$K_c^2=-\kappa^2\left(\frac{2i\alpha}{U_g\kappa}+\left(\frac{\alpha}{U_g\kappa}\right)^2\right). \tag{47}$$

The solutions of the liquid motion equations (40), (41), which vanish at infinity and also satisfy the boundary conditions equations (34), (35) at the gas–liquid interface, are

$$\psi_1=V_i x-\frac{i\alpha(l^2+\kappa^2)}{\kappa(\kappa^2-l^2)}\eta e^{-\kappa(r-a)} \tag{48}$$

and

$$\psi_2=\frac{2i\alpha\kappa}{\kappa^2-l^2}\eta e^{-l(r-a)} \tag{49}$$

where a is the orifice radius, ν is the kinematic viscosity, and

$$l^2=\kappa^2+\frac{\alpha}{\nu}. \tag{50}$$

By substituting equation (48) and equations (43), (44) and then integrating, the pressure in the liquid phase is obtained as

$$P_f=C-\rho\alpha^2\frac{\kappa^2+l^2}{\kappa(\kappa^2-l^2)}\eta e^{-\kappa(r-a)}$$

where C is an integration constant and is evaluated by applying the condition equation (36) at $x=0$ where the disturbance originates and the deviation of η of the gas–liquid interface is zero. By noting that from equation (46), at the location where the disturbance originates, namely at $x=0$, we have

$$P_g=P_o(\text{orifice condition})=\frac{1}{\gamma}\rho_g U_g^2$$

and

$$\frac{\partial\mathbf{V}_f\cdot\mathbf{r}}{\partial r}=0.$$

The solution to the pressure in the liquid phase, equations (43), (44), is found as

$$P_f=\frac{1}{\gamma}\rho_g U_g^2-\frac{\sigma}{a}+\dot{m}_{\text{evap}}(V_g-V_f)-\rho\alpha^2\frac{(l^2+\kappa^2)}{\kappa(\kappa^2-l^2)}\eta(x,t). \tag{51}$$

Substituting equation (46) into equation (30) yields

$$P_g = \frac{1}{\gamma}\rho_g U_g^2 - \rho_g(\alpha + i\kappa U_g)^2 \frac{\sin(K_c r)}{K_c \cos(K_c a)}\eta(x,t) + \rho_g V_1\left[-V_1 + (\alpha + i\kappa U_g)\frac{\cos(K_c r)}{\cos(K_c a)}\eta(x,t)\right]. \quad (52)$$

By using the asymptotic formulas at the interface ($r = a$),

$$\cos(K_c a) \approx \frac{1}{2}e^{iK_c a}; \quad \sin(K_c a) \approx \frac{1}{2i}e^{iK_c a}.$$

The gas-pressure equation (52) at the interface can be simplified as

$$P_g = \frac{1}{\gamma}\rho_g U_g^2 + i\rho_g \frac{(\alpha + i\kappa U_g)^2}{K_c}\eta + \rho_g V_1(\alpha + i\kappa U_g)\eta. \quad (53)$$

With the above solutions, the dispersion equation at the interfacial boundary $r = a$ is found, by substituting equations (45), (51), and (53) into equation (36) and using equations (38), (42), (48), and (49), as

$$\frac{\alpha^2(\kappa^2 + l^2)}{\kappa^2 - l^2} + 2\nu\alpha\kappa^2\frac{(\kappa^2 - l^2)}{\kappa^2 - l^2} + i\frac{\rho_g\kappa}{\rho K_c}(i\kappa U_g + \alpha)^2 + \frac{\rho_g}{\rho}V_1\kappa(i\kappa U_g + \alpha) = \frac{\sigma\kappa^3}{\rho}. \quad (54)$$

6. SOLUTIONS OF THE DISPERSION EQUATION

For ease in obtaining the roots of equation (54), the equation is to be separated into the real and the imaginary parts. By substituting l and K_c from equations (47) and (50), and splitting α into the time amplification factor (α_r) and the angular frequency of wave disturbance (α_i), $\alpha = \alpha_r - i\alpha_i$, the dispersion equation is separated into real and imaginary parts as

$$-4\kappa^2\nu\alpha_r + \alpha_i^2 - \alpha_r^2 - 4\nu^2\kappa^4 + \frac{1}{2}\frac{\rho_g}{\rho}(\kappa U_g)^{5/2} \times \left(\frac{(\alpha_i^2 + \alpha_r^2)^{1/2} + \alpha_i}{\alpha_i^2 + \alpha_r^2}\right)^{1/2} + 2^{3/2}\kappa^3\nu^2\left\{\left[\left(\kappa^2 + \frac{\alpha_r}{\nu}\right)^2 + \left(\frac{\alpha_i}{\nu}\right)^2\right]^{1/2} + \left(\kappa^2 + \frac{\alpha_r}{\nu}\right)\right\}^{1/2} = \frac{\alpha\kappa^3}{\rho} \quad (55)$$

$$4\kappa^2\nu\alpha_i + 2\alpha_i\alpha_r + \frac{\rho_g}{\rho}V_1\kappa^2 U_g - 2^{3/2}\nu^2\kappa^3\left\{\left[\left(\kappa^2 + \frac{\alpha_r}{\nu}\right)^2 + \left(\frac{\alpha_i}{\nu}\right)^2\right]^{1/2} - \left(\kappa^2 + \frac{\alpha_r}{\nu}\right)\right\}^{1/2} - \frac{1}{2}\frac{\rho_g}{\rho}(\kappa U_g)^{5/2}\left(\frac{(\alpha_i^2 + \alpha_r^2)^{1/2} - \alpha_i}{\alpha_i^2 + \alpha_r^2}\right)^{1/2} = 0. \quad (56)$$

For the present interest, the low-viscosity liquid approximation is applicable. The low-viscosity liquid is defined as one for which the following inequality holds [15, 16]:

$$|\alpha| \gg \nu\kappa^2; \quad |l| \gg \kappa. \quad (57)$$

Then equations (55)–(56) can be simplified and cast into the dimensionless forms in accordance to the following dimensionless variables:

$$\kappa^* = \frac{\kappa\sigma^{3/2}}{\mu^{1/2}\rho_g U_g^{5/2}}; \quad \alpha_r^* = \frac{\alpha_r(\mu\sigma)^{1/2}}{\rho_g U_g^{5/2}}; \quad \alpha_i^* = \frac{\alpha_i(\mu\sigma)^{1/2}}{\rho_g U_g^{5/2}}. \quad (58)$$

They are

$$((\alpha_i^*)^2 - (\alpha_r^*)^2) + \tfrac{1}{2}P_1(\kappa^*)^{5/2} \times \left[\frac{((\alpha_i^*)^2 + (\alpha_r^*)^2)^{1/2} + \alpha_i^*}{(\alpha_i^*)^2 + (\alpha_r^*)^2}\right]^{1/2} = P_1(\kappa^*)^3 \quad (59)$$

and

$$2\alpha_i^*\alpha_r^* - \tfrac{1}{2}P_1(\kappa^*)^{5/2} \times \left[\frac{((\alpha_i^*)^2 + (\alpha_r^*)^2)^{1/2} - \alpha_i^*}{(\alpha_i^*)^2 + (\alpha_r^*)^2}\right]^{1/2} = -P_2(\kappa^*)^2 \quad (60)$$

in which P_1 and P_2 parameters are defined as

$$P_1 \equiv \frac{\rho_g U_g^{5/2}\sigma^{-5/2}\mu^{5/2}}{\rho}; \quad P_2 \equiv \frac{\rho_g U_g \mu^2\sigma^{-2}V_1}{\rho}. \quad (61)$$

It is known that instability occurs when the amplification factor α_r is greater than zero. From the interfacial displacement equation (45), as time goes to infinity, the interfacial wave will have infinite value of amplification, which is a state describing the collapse of the jet. The maximum value of the amplification factor α_r of the wave can be obtained by setting $d\alpha_r^*/d\kappa^* = 0$. Differentiating equations (59), (60) with respect to κ, setting $d\alpha_r^*/d\kappa^* = 0$ and eliminating $d\alpha_i^*/d\kappa^*$ between the resulting equations yields the desired dimensionless form as

$$\left[2\alpha_r^* + \tfrac{1}{2}(2\alpha_i^*\alpha_r^* + P_2)\left(\frac{((\alpha_i^*)^2 + (\alpha_r^*)^2)^{1/2} + 2\alpha_i^*}{(\alpha_i^*)^2 + (\alpha_r^*)^2}\right)\right] \times [\tfrac{1}{2}P_1(\kappa^*)^3 - \tfrac{5}{2}((\alpha_r^*)^2 - (\alpha_i^*)^2)] = (\tfrac{1}{2}P_2(\kappa^*)^2 + 5\alpha_i^*\alpha_r^*)\left[2\alpha_i^* + \tfrac{1}{2}(P_1(\kappa^*)^3 + (\alpha_r^*)^2 - (\alpha_i^*)^2)\left(\frac{((\alpha_i^*)^2 + (\alpha_r^*)^2)^{1/2} - 2\alpha_i^*}{(\alpha_i^*)^2 + (\alpha_r^*)^2}\right)\right]. \quad (62)$$

By solving equations (59), (60), and (62) simultaneously, we can obtain α_{rm}^*, α_{im}^*, and κ_m^* corresponding to maximum instability of the interfacial wave. It is noted that they are functions of two parameters P_1 and P_2 only. The resulting dimensionless amplification factor α_{rm}^*, dimensionless angular frequency α_{im}^* and dimensionless wavelength $(\kappa_m^*)^{-1}$ are presented in Figs. 2–4. In those figures with $P_2 = 0$, they reduce to the prior solution [13] for the case without mass transfer at the gas–liquid interface. From Fig. 2 it is interesting to see that a blowing ($P_2 > 0$), say, by evaporation, at the interface acts to enhance the time amplification factor of the disturbance at maximum instability, while the suction

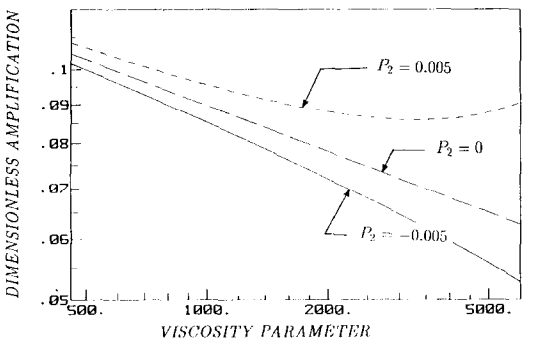

FIG. 2. Dimensionless amplification vs $(1/P_1)$ parameter at different values of parameter.

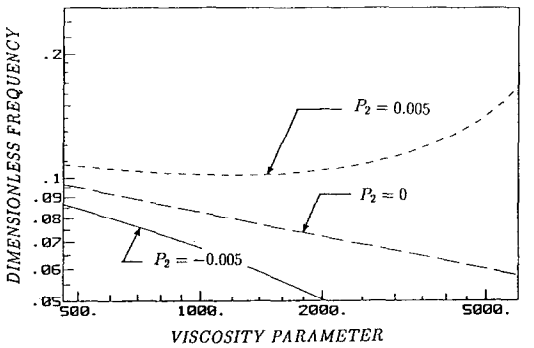

FIG. 3. Dimensionless frequency vs $(1/P_1)$ parameter at different values of diffusion parameter.

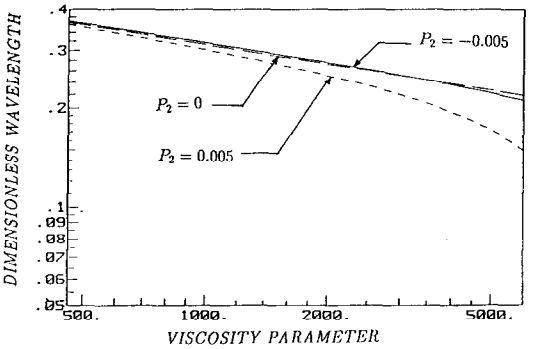

FIG. 4. Dimensionless wavelength vs $(1/P_1)$ parameter at different values of diffusion parameter.

($P_2 < 0$), say, by condensation, acts to reduce the instability. Physically, this appears to be reasonable since a blowing from the interface to gas stream increases the mean axial gas velocity and therefore enhances the instability of the interface while the reverse is true with a suction at the interface. Also, when the surface tension effect increases as compared to the viscous effect (namely, the value of P_1^{-1} increases), the value of the amplification factor decreases whether with or without interfacial mass transfer. Intuitively, the result is correct since surface tension should provide the stability effect. Similar interfacial mass transfer and surface tension effects are found on the disturbance frequency as shown in Fig. 3. However, the effect on the disturbance wavelength is less prevalent (see Fig. 4).

7. PLUME BREAK-OFF LENGTH OF A REACTING SUBMERGED JET

In the design of SCEP (store chemical energy propulsion) for undersea propulsion, a hexafluoride gas (oxidant) is discharged at a choked speed into a combustor filled with liquid lithium (fuel), resulting in a complex reacting submerged jet [1, 2, 4]. Due to the opaqueness of the liquid metal fuel and the metal wall of the combustor, the detailed plume structure of the jet is difficult to measure. To overcome this difficulty, a transparent reacting pair of reactants which have similar reacting characteristics have been chosen to simulate the liquid metal fuel combustion [8]. They injected a sonic hydrochloride gas (oxidant) into an aqueous ammonia solution (fuel). In a series of extensive measurements by varying the ammonia concentration and underexpansion ratio, they discovered that, with the presence of ammonia in the solution, the reacting jet is much less stable than the one without ammonia. In fact the instability caused a break-off of the submerged reacting jet shortly leaving the nozzle to form a detached plume (bubble) as sketched in Fig. 1. It is of interest to see if the results of the present instability analysis can be successfully applied to predict the reported break-off lengths [8].

In the submerged reacting plume, the disturbance on the gas–liquid interface originates at the orifice and its amplitude grows as it propagates downstream. If the plume breaks off, it appears reasonable to assume that it occurs at the axial location where the disturbance reaches its maximum instability. Or, at least, the break-off length can be assumed to be proportional to the distance where the maximum instability occurs. The maximum instability location, which is equivalent to the break-off length here, can be expressed in the following functional form [14]:

$$L_o = \frac{C_o U_g}{\alpha_{rm}}\left[C_L + \ln\left(\left(\frac{\lambda_m}{a}\right)^A \omega^B\right)\right]$$

where

$$\lambda_m = \frac{2\pi}{\kappa_m}; \quad \omega = \frac{|(\alpha_{rm}^2 + \alpha_{im}^2)^{1/2}|}{(\kappa_m U_g)}$$

and C_o, C_L, A and B are empirical constants to be determined experimentally. To determine these constants using the break-off length data of HCl(g)–NH_3(aq) system [8], a determination of the blowing velocity, V_1, and P_2 parameter is needed to solve for the maximum time amplification factor α_{rm}, the maximum frequency α_{im}, and the maximum wavelength λ_m from equations (59), (60), and (62). For each experimental condition/data, V_1 is estimated by the simplified theory of mass transfer method (the

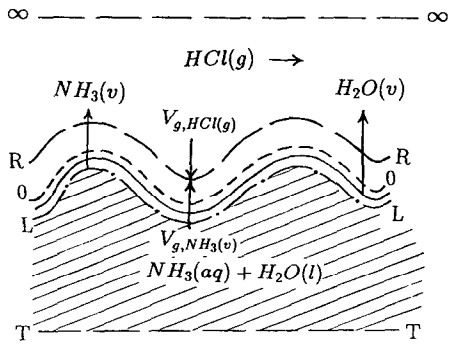

FIG. 5. Control volume and various states at phase change interface with reaction in gas phase.

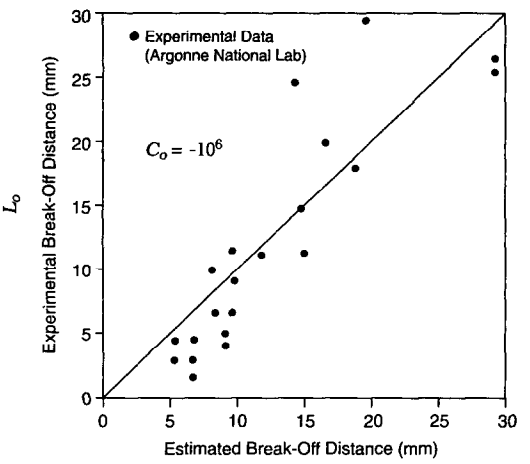

FIG. 6. Break-off point estimation versus experimental data of Cho *et al.* [8].

mass-transfer conductance/driving force concept) based on the work of Spalding (see, for example, [16]). Briefly, by referring to Fig. 5, the blowing velocity is determined from the ammonia gas desorption (evaporation) rate from the aqueous solution. The ammonia gas is assumed to react with HCl gas at the R–R surface according to the following simple stoichiometric reaction:

$$1\,\text{kg}\,(NH_3)_g(\text{fuel}) + r\,\text{kg of}\,(HCl)_g(\text{oxidant}) \rightarrow (1+r)\,\text{kg}\,NH_4Cl\,(\text{product}).$$

The usual assumptions of fast chemistry, equal specific heats and Lewis number of unity are made. Also, no fuel or oxidant remains at the R–R surface, only HCl gas is present at the ∞–∞ plane, and NH_3 vapor and minor trace of water vapor are present at the O–O surface. More details of the estimation procedure can be found in ref. [16]. A least-squares fit through fourteen plume data [8] with different operating conditions as utilized to obtain the empirical constants to yield the equation

$$\frac{L_o \alpha_{rm}}{U_g} = -10^6 \times \ln\left[2.282\left(\frac{\lambda_m}{a}\right)^{0.1533} \omega^{0.0761}\right].$$

The prediction of the break-off plume length based on the above equation is compared in Fig. 6 with all data of more than twenty different experimental conditions. The comparison shows that the trend is correct. Considering the limitation of the linear stability theory, the agreement shown in Fig. 6 is in fact reasonable.

Finally, the result of present analysis shows that evaporation enhances the wave instability. It may explain the experimental findings [8] that periodic plume break-off behavior existed when a HCl gas was injected into an ammonia solution and that a much more stable plume was found when the HCl gas was injected into water without ammonia. This is because in the former, ammonia vapor has to evaporate from the solution to react while in the latter the HCl gas simply dissolved in water like a condensation process.

8. CONCLUSIONS

The effect of mass transfer on the Kelvin–Helmholtz instability of the gas–liquid interface of a sonic gas jet submerged in a liquid has been analyzed. Solutions have been presented for the dimensionless amplification factor, angular frequency and wavelength corresponding to the maximum instability of the interfacial wave. The results show that the interfacial evaporation or exothermic reaction enhances the wave instability while the condensation or endothermic reaction reduces the instability. The results also elucidate the periodic break-off phenomena observed in reacting submerged jets. Finally, application to the prediction of the break-off length has been made and theoretical predictions are found in satisfactory agreement to experimental data.

REFERENCES

1. U. K. P. Biermann, The lithium/sulphurhexafluoride heat source in combination with a Stirling engine as an environmental independent underwater propulsion system, *Proc. of Tenth Intersociety Energy Conf.*, pp. 1023–1030 (1975).
2. S. H. Chan and M. M. M. Abou-Ellail, Multi-fluid model of turbulence for Li–SF_6 submerged combustion, *AIAA J.* **31**, 1526–1929 (1983).
3. E. G. Groff and G. M. Faeth, A steady metal combustor as a closed thermal energy source, *J. Hydronautics* **2**, 63–70 (1978).
4. T. G. Hughes, R. B. Smith and D. H. Kiley, Stored chemical energy propulsion system for underwater applications, *J. Energy* **7**, 128–133 (1983).
5. J. N. Mattavi, F. E. Heffner and A. A. Miklos, The Stirling engine for underwater vehicle applications, *SAE Trans.* **78**(4), 2376–2400 (1969).
6. E. O. Hoefele and J. K. Brimacombe, Flow regimes in submerged gas injection, *Met. Trans. B* **10B**, 631–648 (1979).
7. D. Greene, Summary of small and intermediate sodium/water reaction programs in the United States, *Proc. of the 22nd IECEC*, Vol. 3, pp. 1630–1637 (1987).

8. D. H. Cho, D. R. Armstrong and L. Bova, Experimental study of reacting gas jets in liquids: heat release effects, *Chem. Engng Sci.* **45**(2), 423–435 (1990).
9. I. D. Chang and P. E. Russel, Stability of a liquid adjacent to high-speed gas stream, *Phys. Fluids* **8**(6), 1018–1026 (1965).
10. P. R. Nachtscheim, Stability of crosshatched wave patterns in thin liquid films adjacent to supersonic streams, *Phys. Fluids* **13**(13), 2432–2447 (1970).
11. A. H. Nayfeh and W. S. Saric, Non-linear Kelvin–Helmholtz instability, *Fluid Mech.* **46,** 209–231 (1971).
12. A. D. D. Craik, Wind-generated waves in thin liquid films, *Fluid Mech.* **26,** 369–392 (1966).
13. T. C. Chawla, The Kelvin–Helmholtz instability of the gas–liquid interface of a sonic gas jet submerged in a liquid, *J. Fluid Mech.* **67**(3), 513–537 (1975).
14. T. C. Chawla, Rate of liquid entrainment at the gas–liquid interface of a liquid submerged sonic gas jet, *Nucl. Sci. Engng* **56,** 1–6 (1975).
15. T. C. Chawla, Liquid-entrainment rate and droplet size relative to potential fuel-failure propagation due to fission-gas jet impingement in LMFBR subassemblies, ANL-7949, *Reactor Technol.*, Argonne National Laboratory (1972).
16. W. M. Kays and M. E. Crawford, *Convective Heat and Mass Transfer* (2nd Edn), pp. 332–383. McGraw-Hill, New York (1980).